Electron Microscopy and Spectroscopy Investigation of Atomic, Electronic, and Phonon Structures of $NdNiO_2/SrTiO_3$ Interface

Yuan Yin(尹源)[1†], Mei Wu(武媚)[1†], Xiang Ding(丁翔)[2†], Peiyi He(何沛一)[1†], Qize Li(李其泽)[1,3], Xiaowen Zhang(张潇文)[1], Ruixue Zhu(朱锐雪)[1], Ruilin Mao(毛瑞麟)[1], Xiaoyue Gao(高晓悦)[1], Ruochen Shi(时若晨)[1*], Liang Qiao(乔梁)[2*], and Peng Gao(高鹏)[1,4,5*]

[1]*International Center for Quantum Materials, and Electron Microscopy Laboratory, School of Physics, Peking University, Beijing 100871, China*
[2]*School of Physics, University of Electronic Science and Technology of China, Chengdu 611731, China*
[3]*Department of Physics, University of California at Berkeley, Berkeley, CA 94720, USA*
[4]*Interdisciplinary Institute of Light-Element Quantum Materials and Research Center for Light-Element Advanced Materials, Peking University, Beijing 100871, China*
[5]*Collaborative Innovation Center of Quantum Matter, Beijing 100871, China*

(Received 9 December 2024; accepted manuscript online 7 March 2025)

The infinite-layer nickelates, proposed as analogs to superconducting cuprates, provide a promising platform for exploring the mechanisms of unconventional superconductivity. However, the superconductivity has been exclusively observed in thin films under atmospheric pressure, underscoring the critical role of the heterointerface. Here, we employed the advanced scanning transmission electron microscopy-electron energy loss spectroscopy technique to thoroughly investigate the atomic configuration, layer-resolved electronic states and phonon modes across the $NdNiO_2/SrTiO_3$ interface. Our findings reveal that interfacial Sr diffusion drives the formation of a p-type interface, thus facilitating hole doping into the oxygen and nickel bands. Notably, a pronounced redshift of the highest-energy optical phonon of $NdNiO_2$ (~ 78 meV) is observed at the interface, predominantly induced by Sr diffusion and epitaxial strain. Our work demonstrates that interfacial Sr diffusion and epitaxial strain can reconfigure the electronic and phonon structures at the p-type interface, offering critical insights for elucidating the superconducting mechanisms in infinite-layer nickelates.

DOI: 10.1088/0256-307X/42/4/047402 CSTR: 32039.14.0256-307X.42.4.047402

In 1999, it was theoretically predicted that nickelates featuring spin $S = 1/2$ Ni^+ in planar Ni-O structures could exhibit magnetic insulating behavior, with the doped state Ni^{2+} ($S = 0$) analogous to that of Cu^{3+} ($S = 0$) in hole-doped cuprates.[1] Two decades later, the experimental discovery of superconductivity in infinite-layer nickelates, with critical temperatures (T_c) ranging from 9 to 15 K, sparked widespread interest.[2] Infinite-layer nickelates share several key similarities with cuprates. Both systems possess $3d^9$ electron configuration in their undoped states, with the $3d_{x^2-y^2}$ band being the dominant one.[3,4] However, notable differences exist between the two materials. Cuprates are classified within the charge-transfer regime, whereas infinite-layer nickelates fall under the Mott–Hubbard regime,[5] resulting in weaker hybridization between O 2p and Ni 3d orbitals than that between O 2p and Cu 3d orbitals.[6,7] Additionally, unlike cuprates, infinite-layer nickelates exhibit a multi-band character with a "self-doping" effect,[3,8] and lack long-range magnetic ordering at low temperatures.[9]

These similarities and differences have sparked controversies surrounding the pairing mechanism behind high-temperature superconductivity,[8,10,11] long-range antiferromagnetic order,[12,13] charge order,[14–16] Kondo effect,[17] and interfacial effects[18–20] of nickelates. Among these, the interfacial effect has always been a contentious question,[18–20] as bulk and powder infinite-layer nickelates have yet to exhibit superconductivity under atmospheric pressure.[18,21] Theoretical studies indicate that nickelate interfaces with varying configurations display distinct electronic structures,[20,22] and both atomic and electronic reconstructions are inevitable at polar interfaces.[23] Experimentally, the superconducting transition temperature of infinite-layer nickelates has been shown to vary with film thickness[24] and substrates with different compressive strain.[25] These findings naturally raise questions about whether the interface plays a decisive role in the superconductivity of infinite-layer nickelates. Therefore, it is crucial to clarify the impact of the interface from a microscopic perspective and uncover its role in superconductivity. Traditional experimental techniques, such as X-ray absorption spectroscopy (XAS) and resonant inelastic X-ray spectroscopy (RIXS), are limited to resolve interface-specific contributions due to insufficient spatial

†These authors contributed equally to this work.
*Corresponding author. Email: shirc1993@pku.edu.cn; liang.qiao@uestc.edu.cn; pgao@pku.edu.cn
© 2025 Chinese Physical Society and IOP Publishing Ltd. All rights, including for text and data mining, AI training, and similar technologies, are reserved.

resolution. Herein, we utilize the advanced scanning transmission electron microscopy-electron energy loss spectroscopy (STEM-EELS) to probe the atomic, electronic, and phonon structures at the interface with high precision.

In this study, we identify a p-type interface characterized by the intermixing of A-site atoms, resulting in the formation of stoichiometric $Nd_{1-x}Sr_xNiO_2$ near the interface, which effectively induces hole doping.[26] STEM-EELS results reveal that the holes are partly doped into the 3d orbitals of nickel and partly into the 2p orbitals of oxygen, corresponding to a joint final state of $3d^8$ and $3d^9\underline{L}$, where $\underline{L}$ denotes a ligand hole. Additionally, a pronounced redshift in the highest-energy optical phonon (HEOP) of $NdNiO_2$ (~ 78 meV) is observed at the interface, primarily driven by Sr diffusion and epitaxial strain, as supported by theoretical calculations. These results indicate that the $SrTiO_3$ substrates facilitates hole doping into $NdNiO_2$ films, analogous to the interfacial superconductivity observed in $CaCuO_2/SrTiO_3$ systems.[27,28] Moreover, the interfacial interaction induces a HEOP softening in $NdNiO_2$. Our findings highlight the capability to precisely correlate the atomic structure, electronic states, and phonon structure, thus enhancing the understanding of the underlying mechanism in nickel-based superconductors.

Infinite-layer nickelates thin films without capping layers were prepared on $SrTiO_3$ (001) substrates by pulsed laser deposition and topotactic reduction (see Supplementary Methods for details), with the corresponding electrical measurement shown in Fig. S1. The high-angle annular dark-field (HAADF) image and annular bright-field (ABF) image are shown in Figs. 1(a) and 1(b) to reveal the configuration near the interface. The elemental maps of energy dispersive X-ray spectroscopy (EDS) with atomic resolution in Fig. 1(c) depict the spatial distribution of Nd, Sr, Ni, and Ti atoms, confirming elemental intermixing at the interface. Unlike previous reports of B-site atoms (Ni and Ti) mixing,[20] this study identifies intermixing of A-site atoms (Nd and Sr), with Sr being the dominant one. This difference is attributed to the distinct termination surface of the $SrTiO_3$ substrate, which in this case is SrO-terminated, favoring the formation of a p-type interface with A-site atom mixing. The integral line profiles of the corresponding elements are shown in Fig. 1(d), where layer 0, indicated by the arrow, is the pronounced mixing layer of Nd and Sr. Notably, no significant diffusion of Ti or Ni is observed in Figs. 1(c) and 1(d). Based on these results, the atomic configuration across the interface is schematically illustrated in the inset of Fig. 1(b). The presence of apical oxygen in the intermixing layer results in a pyramidal Ni-O configuration closest to the interface, different from the planar tetragonal Ni-O configuration observed in other layers. This structural variation leads to a distinct coordination environment in the interfacial layer. To delve into the strain near the interface, we performed peak fitting of the A-site atom positions in the HAADF images and calculated the scaled lattice parameter using $SrTiO_3$ far away from the interface as a reference, as shown in Fig. 1(e). The in-plane scaled lattice parameter exhibits minor variation, while the out-of-plane one undergoes significant changes within the first two unit cells near the interface. The out-of-plane compressive strain of $NdNiO_2$ near the interface is approximately 2.6% relative to unstrained bulk $NdNiO_2$.

Here, the observed intermixing layer of Nd and Sr is anticipated to alleviate the "polarization catastrophe", as illustrated in Supplemental Material, Figs. S2(a) and S2(b). This atomic reconstruction at the interface suppresses potential divergence, thereby excluding the influence of the electric field on the electronic structure,[20] which will not be discussed in the following analyses. Meanwhile, this intermixing effectively acts as Sr-doping into $NdNiO_2$, inducing hole doping. As the distance from the interface increases, the concentration of doped holes decreases due to the declining Sr concentration, leading to electronic structure modifications as expected.

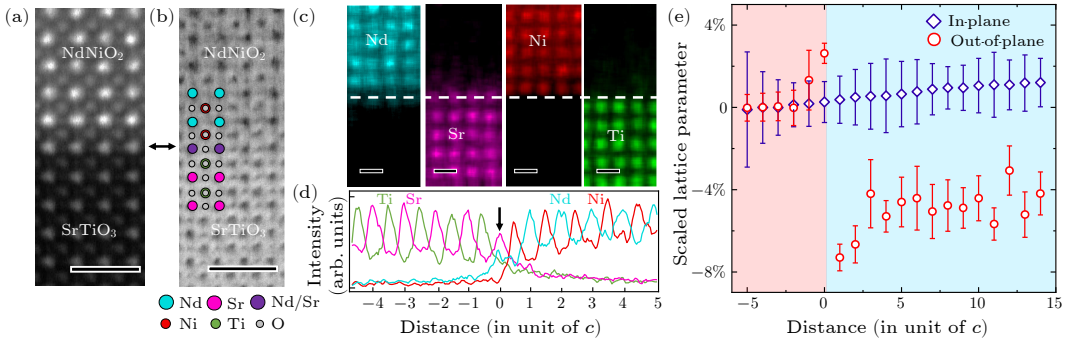

Fig. 1. The atomic structure and strain of $NdNiO_2/SrTiO_3$. (a) The HAADF and (b) ABF images of $NdNiO_2$ on $SrTiO_3$ substrate, where the schematic diagram of atomic structure is illustrated according to image contrast and EDS results. The scale bar is 1 nm. (c) The EDS of Nd, Sr, Ni and Ti across the interface with atomic resolution. The scale bar is 5 Å. Intermixing of Nd and Sr (white line) occurs at the layer indicated by the bidirectional arrow layer between (a) and (b). (d) The Nd, Sr, Ni, Ti intensity line profiles of EDS across the interface. The arrow indicates the position of intermixing layer. (e) The in-plane and out-of-plane scaled lattice parameters. The error bars are the standard deviation (s.d.).

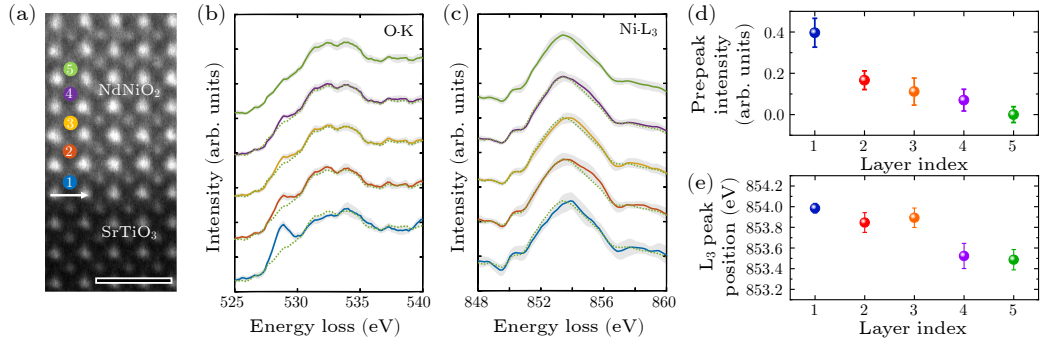

Fig. 2. Atomic-resolution O-K edge and Ni-L_3 peak spectra near the interface. (a) A STEM-HAADF image of the $NdNiO_2/SrTiO_3$ interface, the white arrow indicates the intermixing layer, and five layers away from the interface are marked with numbered colorful dots, referring to layer 1 to 5 respectively. The scale bar is 1 nm. (b) The O-K edge and (c) Ni-L_3 peak of the corresponding five layers, the gray shadow is the standard deviation (s.d.) of the spectral lines and the dotted lines mark the characteristics of layer 5 for better comparison. (d) The O-K pre-peak intensity integrated from 528 to 530 eV relative to layer 5 and (e) the Ni-L_3 peak position of five layers. Error bars represent s.d.

To investigate the changes in the electronic structures near the interface, we acquired the layer-resolved energy-loss near-edge fine structure (ELNES) of the first five layers of $NdNiO_2$ adjacent to the interface. Figure 2(a) displays a HAADF image of the five interfacial layers labeled by colored dots numbered from 1 to 5. The O-K edge spectra in Fig. 2(b) reveal significant variations across these layers. For clarity, the O-K edge spectrum of layer 5 (represented by a dashed green line) was shifted to align with the spectra of other layers. Notably, the O-K edge of layer 1 exhibits a distinct pre-peak at approximately 528.8 eV, with its intensity gradually diminishing as the distance from the interface increases. From the third layer onward, this pre-peak transforms into a shoulder and nearly disappears by layer 5, consistent with the characteristics of bulk $NdNiO_2$ reported in previous studies.[20,29] Figure 2(d) demonstrates that the additional intensity, integrated from 528 to 530 eV relative to layer 5, gradually decreases from layer 1 to layer 4. The pre-peak of the O-K edge reflects the degree of hybridization between O 2p and transition metal orbitals.[30,31] This feature is prominent in perovskite $NdNiO_3$, where Ni adopts a $3d^7\underline{L}$ ground state in the metallic phase, but it nearly vanishes in the bulk infinite-layer $NdNiO_2$, where Ni is in a $3d^9$ state.[19,29] Therefore, the appearance of the pre-peak suggests the presence of a $3d^9\underline{L}$ state, most likely induced by Sr diffusion at the interface, which facilitates hole doping.

Similarly, the Ni-L_3 spectral line of layer 5 was overlaid onto the spectra of other layers for comparison in Fig. 2(c), and the corresponding L_3 peak positions for each layer were extracted, as shown in Fig. 2(e). The L_3 peak exhibits a blue shift when moving closer to the interface, with the peak of layer 1 shifting by nearly 0.5 eV relative to layer 5. This indicates an increase in the valence state of Ni and a tendency toward $3d^8$ state near the interface. It is worth noting that the peak position shift is neither linear nor monotonic, consistent with previous reports.[29] Additionally, the main peak gradually broadens from layer 5 to layer 2, accompanied by the emergence of a high-energy shoulder, which is particularly prominent in layer 2. This spectral feature aligns with XAS[7] and EELS[29] results for $NdNiO_2$ superconducting samples with varying Sr doping, reflecting hybridization between the O 2p and Ni 3d orbitals. Similar high-energy shoulder features have been observed in the XAS spectra of superconducting cuprates and are attributed to ligand hole states.[27,32–34] The atomic configuration of $Nd_{1-x}Sr_xNiO_{2.5}$ (where the excess $O_{0.5}$ originates from the apical oxygen atoms of the interfacial layer) at the interface in Fig. 1(b) further increases the valence state of Ni, resulting in an additional blueshift of layer 1. The complete $L_{2,3}$ edges of Ni are presented in Fig. S3(b). Additionally, the $M_{4,5}$ edges of Nd were investigated, as shown in Fig. S3(c). No distinguishable energy shifts or shape changes were observed, indicating that the 4f electronic state of the rare earth element Nd exhibits low sensitivity to such local atomic or electronic reconstructions.[19] To understand the effect of strain on the electronic structure, we have performed the density functional theory (DFT) calculations, as shown in Fig. S4. The results reveal that the shift in the partial density of states of $NdNiO_2$ under 2.6% strain near the Fermi surface is negligible, thus the influence of strain on the electronic structure can be ruled out here. These findings confirm that interfacial Sr diffusion effectively induces hole doping, leading to the formation of $3d^8$ and $3d^9\underline{L}$ states.

Electron–phonon coupling (EPC) has been considered to play a role in conventional[35] and high-temperature superconductivity.[36,37] Several previous studies based on DFT calculations suggested that the EPC was too weak to contribute to the superconductivity in infinite-layer nickelates.[38–41] However, a recent work employing ab initio GW theory has proposed that the EPC contributes significantly to the superconducting temperature of infinite-layer nickelates.[42] This discrepancy highlights the importance of experimentally investigating phonon behavior near the interface. However, due to the lack of Raman activity in the structure of $NdNiO_2$,[43] phonon-related experiments have been rarely reported in this system, not to mention the knowledge of the phonon spectrum near the interface. To fill this gap, we measured the phonon spectrum near the $NdNiO_2/SrTiO_3$ interface [Fig. 3(b)] with

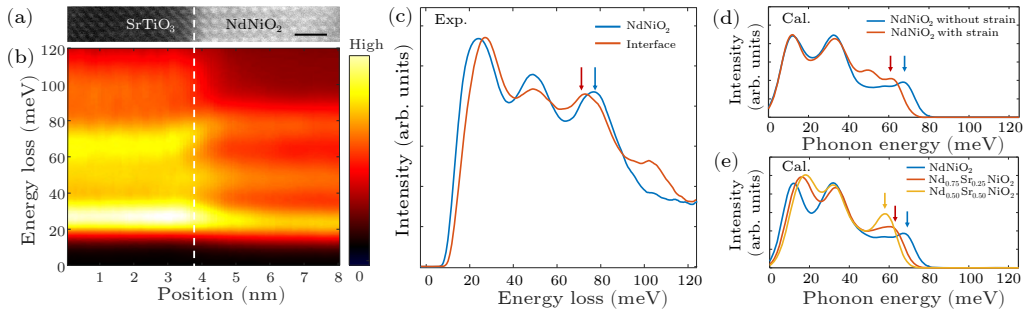

Fig. 3. The measured and calculated phonon spectra across the $NdNiO_2/SrTiO_3$ interface. (a) The HAADF image showing the interfacial region of measurement, the scale bar is 1 nm. (b) The phonon mapping of $NdNiO_2/SrTiO_3$, where the interface is labeled by the dashed line. (c) The extracted phonon spectra of $NdNiO_2$ (blue) and the interface (red). (d) The convolution results of calculated PDOS for bulk $NdNiO_2$ without (blue) and under 2.6% out-of-plane strain (red) with a Gaussian peak of 10 meV full width at half maximum (FWHM). (e) The convolution results of calculated PDOS for $NdNiO_2$ (blue), $Nd_{0.75}Sr_{0.25}NiO_2$ (red) and $Nd_{0.50}Sr_{0.50}NiO_2$ (yellow) with a Gaussian peak of 10 meV FWHM.

the corresponding HAADF image of the acquisition region [Fig. 3(a)], where the white dashed line refers to the interface position. The phonon spectra of bulk $NdNiO_2$ (blue) and the interface (red), extracted from the EEL spectrum, are presented in Fig. 3(c). The highest-energy optical phonon (HEOP) of $NdNiO_2$ ($\sim$78 meV) exhibits a pronounced redshift near the interface (indicated by the shift from the blue arrow to the red arrow). As mentioned, there are epitaxial strain and Sr diffusion at the interface. Therefore, to investigate the effects of both factors on the HEOP in $NdNiO_2$, we performed density functional perturbation theory (DFPT) calculations for the phonon of $NdNiO_2$ under 2.6% out-of-plane strain and $Nd_{1-x}Sr_xNiO_2$ ($x = 0,\ 0.25,\ 0.5$) without strain. The phonon dispersions and phonon density of states (PDOS) of $NdNiO_2$ with and without strain are shown in Fig. S5, and the eigenvectors of the HEOP are presented in Fig. S6. For a better comparison with the experimental results, we convoluted the PDOS of $NdNiO_2$ with/without strain and $Nd_{1-x}Sr_xNiO_2$ ($x = 0,\ 0.25,\ 0.5$) with a Gaussian peak of 10 meV full width at half maximum (FWHM) to simulate the instrumental broadening, as shown in Figs. 3(d) and 3(e) respectively. The slight discrepancy in phonon energy between calculation and experiment is likely due to the inherent limitations of DFT. Nevertheless, the calculation results should correctly reflect the main feature for the phonon energy changes. In Fig. 3(d), the HEOP of $NdNiO_2$ under 2.6% out-of-plane strain shows an evident redshift while other phonon modes remain largely unchanged compared to the bulk. Similarly, in Fig. 3(e), the HEOP of $Nd_{1-x}Sr_xNiO_2$ shifts to lower energy with increasing Sr doping, whereas the lowest-energy phonon mode shifts to higher energy. These results demonstrate that both strain and Sr diffusion contribute to the optical phonon softening near the interface, while the influence of electron-phonon coupling should not be underestimated as well.[42]

$NdNiO_2$ is the parent oxide to $Nd_{1-x}Sr_xNiO_2$, which exhibits superconductivity when Sr doping concentration x ranges from 10% to 25%.[44,45] Therefore, the doping concentration plays a critical role in the emergence of superconductivity. For $NdNiO_2$ films grown on $SrTiO_3$ substrates, our experimental results reveal that the Sr gradually diffuses into the film in such p-type interface. The electronic structures of the $NdNiO_2$ films within 1–2 unit cells near the interface are consistent with those of superconducting $Nd_{0.775}Sr_{0.225}NiO_2$ reported in previous study.[29] This suggests that Sr diffusion from the substrate can serve as a source of doping holes, and regions with doping concentrations falling within the superconducting dome can exhibit superconducting properties. Recent experiments have reported superconductivity in parent infinite-layer nickelates.[46,47] Regarding the underlying mechanisms, it should be noted that the potential elemental diffusion from the capping layer might also exert an influence on the superconductivity. Therefore, the STEM-EELS technique is superb for mechanism studies at atomic scale in this system. We hope this work can provide valuable insights for the understanding of the underlying mechanisms in nickel-based superconductivity.

Given that the region affected by Sr diffusion is relatively small compared to the entire $NdNiO_2$ film, this could present challenges for macroscopic superconductivity measurements. One promising strategy is to fabricate $(NdNiO_2)_m/(SrTiO_3)_n$ superlattices with proper relative thickness of $NdNiO_2$ and $SrTiO_3$, thereby increasing the proportion of such doped region. A previous experiment has successfully achieved superconductivity with T_c = 40 K in $(CaCuO_2)_m/(SrTiO_3)_n$ superlattices.[27] Subsequent EELS results demonstrated that oxygen are incorporated into the Ca plane at the $CaCuO_2/SrTiO_3$ interface, serving as apical oxygen for Cu and introducing holes into the CuO_2 planes, thus enhancing superconductivity.[28] These experimental results align with our observation of Sr-induced hole doping at the $NdNiO_2/SrTiO_3$ interface. Therefore, $(NdNiO_2)_m/(SrTiO_3)_n$ superlattices remain to be fabricated and are well worth for further exploring.

As previously discussed, Sr diffusion, combined with epitaxial strain, significantly modifies the electronic and phonon structures of the $NdNiO_2$ film at the interface. However, such a p-type interface induced by Sr diffusion has been rarely reported in prior studies on $NdNiO_2$ thin

films. Our findings can inspire the interfacial elemental modulation of infinite-layer nickelates superconductivity. Meanwhile, research has demonstrated that infinite-layer nickelates grown on substrates with different compressive strains exhibit diverse superconducting transition temperatures.[25] Several studies on Ruddlesden-Popper phase have achieved T_c up to 80 K under high-pressure conditions.[48,49] However, these studies primarily focused on the impact of strain on the electronic structure, overlooking its effects on phonon properties.[49] Our results reveal that 2.6% epitaxial strain at the interface has a negligible effect on the electronic structure but contributes to phonon softening in infinite-layer nickelates. Consequently, strain engineering can offer an effective approach for designing interfaces with tailored phonon properties, opening new avenues for exploring potential mechanisms to enhance superconductivity.

In summary, we have investigated the p-type $NdNiO_2/SrTiO_3$ interface and demonstrated that elemental intermixing and epitaxial strain at the interface can reshape the electronic and phonon structures. The Sr diffusion from the substrates, serving as a hole source, can introduce gradient hole doping into the films. Layer-resolved O-K edge and Ni-L_3 edge spectra reveal that the doped holes occupy both O 2p and Ni 3d orbitals, distinguishing infinite-layer nickelates from charge-transfer cuprates and showing multiband character.[29] Additionally, a redshift in the highest-energy optical phonon of the $NdNiO_2$ film at the interface was observed, primarily driven by Sr diffusion and epitaxial strain, as confirmed by comparisons between DFPT calculations and experimental results. Our atomic-scale study could be essential for elucidating macroscopic experimental phenomena in infinite-layer nickelates and advancing the understanding of superconductivity mechanisms.

Acknowledgements. The work was supported by the National Natural Science Foundation of China [52125307 (to P.G.), 12404192 (to R.C.S), 12274061 (to L. Q.)]. L.Q. acknowledges Key Research and Development Program from the Ministry of Science and Technology (2023YFA1406301). P.G. acknowledges the support from the New Cornerstone Science Foundation through the XPLORER PRIZE. We acknowledge Electron Microscopy Laboratory of Peking University for the use of electron microscopes. We acknowledge the High-performance Computing Platform of Peking University for providing computational resources for the DFT and DFPT calculation.

References

[1] Anisimov V I, Bukhvalov D, and Rice T M 1999 *Phys. Rev. B* **59** 7901

[2] Li D, Lee K, Wang B Y, Osada M, Crossley S, Lee H R, Cui Y, Hikita Y, and Hwang H Y 2019 *Nature* **572** 624

[3] Karp J, Botana A S, Norman M R, Park H, Zingl M, and Millis A 2020 *Phys. Rev. X* **10** 021061

[4] El-Moudny S, Lmouchter M, and Zidouh H 2023 *Comp. Mater. Sci.* **221** 112082

[5] Zaanen J, Sawatzky G A, and Allen J W 1985 *Phys. Rev. Lett.* **55** 418

[6] Hepting M, Li D, Jia C J, Lu H, Paris E, Tseng Y, Feng X, Osada M, Been E, Hikita Y, Chuang Y D, Hussain Z, Zhou K J, Nag A, Garcia-Fernandez M, Rossi M, Huang H Y, Huang D J, Shen Z X, Schmitt T, Hwang H Y, Moritz B, Zaanen J, Devereaux T P, and Lee W S 2020 *Nat. Mater.* **19** 381

[7] Rossi M, Lu H, Nag A, Li D, Osada M, Lee K, Wang B Y, Agrestini S, Garcia-Fernandez M, Chuang Y D, Shen Z X, Hwang H Y, Moritz B, Zhou K J, Devereaux T P, and Lee W S 2021 *Phys. Rev. B* **104** L220505

[8] Sakakibara H, Usui H, Suzuki K, Kotani T, Aoki H, and Kuroki K 2020 *Phys. Rev. Lett.* **125** 077003

[9] Katukuri V M, Bogdanov N A, Weser O, van den Brink J, and Alavi A 2020 *Phys. Rev. B* **102** 241112

[10] Gu Q, Li Y, Wan S, Li H, Guo W, Yang H, Li Q, Zhu X, Pan X, Nie Y, and Wen H H 2020 *Nat. Commun.* **11** 6027

[11] Ji H, Liu Y, Li Y, Ding X, Xie Z, Ji C, Qi S, Gao X, Xu M, Gao P, Qiao L, Yang Y, Zhang G M, and Wang J 2023 *Nat. Commun.* **14** 7155

[12] Liu Z, Ren Z, Zhu W, Wang Z, and Yang J 2020 *npj Quantum Mater.* **5** 31

[13] Leonov I, Skornyakov S L, and Savrasov S Y 2020 *Phys. Rev. B* **101** 241108

[14] Tam C C, Choi J, Ding X, Agrestini S, Nag A, Wu M, Huang B, Luo H, Gao P, García-Fernández M, Qiao L, and Zhou K J 2022 *Nat. Mater.* **21** 1116

[15] Rossi M, Osada M, Choi J, Agrestini S, Jost D, Lee Y, Lu H, Wang B Y, Lee K, Nag A, Chuang Y D, Kuo C T, Lee S J, Moritz B, Devereaux T P, Shen Z X, Lee J S, Zhou K J, Hwang H Y, and Lee W S 2022 *Nat. Phys.* **18** 869

[16] Parzyck C T, Gupta N K, Wu Y, Anil V, Bhatt L, Bouliane M, Gong R, Gregory B Z, Luo A, Sutarto R, He F, Chuang Y D, Zhou T, Herranz G, Kourkoutis L F, Singer A, Schlom D G, Hawthorn D G, and Shen K M 2024 *Nat. Mater.* **23** 486

[17] Zhang G M, Yang Y, and Zhang F C 2020 *Phys. Rev. B* **101** 020501

[18] Li Q, He C, Si J, Zhu X, Zhang Y, and Wen H H 2020 *Commun. Mater.* **1** 16

[19] Raji A, Krieger G, Viart N, Preziosi D, Rueff J P, and Gloter A 2023 *Small* **19** 2304872

[20] Goodge B H, Geisler B, Lee K, Osada M, Wang B Y, Li D, Hwang H Y, Pentcheva R, and Kourkoutis L F 2023 *Nat. Mater.* **22** 466

[21] Wang B X, Zheng H, Krivyakina E, Chmaissem O, Lopes P P, Lynn J W, Gallington L C, Ren Y, Rosenkranz S, Mitchell J F, and Phelan D 2020 *Phys. Rev. Mater.* **4** 084409

[22] Bernardini F and Cano A 2020 *J. Phys. Mater.* **3** 03LT01

[23] He R, Jiang P, Lu Y, Song Y, Chen M, Jin M, Shui L, and Zhong Z 2020 *Phys. Rev. B* **102** 035118

[24] Zeng S W, Yin X M, Li C J, Chow L E, Tang C S, Han K, Huang Z, Cao Y, Wan D Y, Zhang Z T, Lim Z S, Diao C Z, Yang P, Wee A T S, Pennycook S J, and Ariando A 2022 *Nat. Commun.* **13** 743

[25] Ren X, Li J, Chen W C, Gao Q, Sanchez J J, Hales J, Luo H, Rodolakis F, McChesney J L, Xiang T, Hu J, Comin R, Wang Y, Zhou X, and Zhu Z 2023 *Commun. Phys.* **6** 341

[26] Nakagawa N, Hwang H Y, and Muller D A 2006 *Nat. Mater.* **5** 204

[27] Di Castro D, Salvato M, Tebano A, Innocenti D, Aruta C, Prellier W, Lebedev O I, Ottaviani I, Brookes N B, Minola M, Moretti Sala M, Mazzoli C, Medaglia P G, Ghiringhelli G, Braicovich L, Cirillo M, and Balestrino G 2012 *Phys. Rev. B* **86** 134524

[28] Di Castro D, Cantoni C, Ridolfi F, Aruta C, Tebano A, Yang N, and Balestrino G 2015 *Phys. Rev. Lett.* **115** 147001

[29] Goodge B H, Li D, Lee K, Osada M, Wang B Y, Sawatzky G A, Hwang H Y, and Kourkoutis L F 2021 *Proc. Natl. Acad. Sci. U.S.A.* **118** e2007683118

[30] Haruta M, Fujiyoshi Y, Nemoto T, Ishizuka A, Ishizuka K, and Kurata H 2018 *Phys. Rev. B* **97** 205139

[31] Gauquelin N, Benckiser E, Kinyanjui M K, Wu M, Lu Y, Christiani G, Logvenov G, Habermeier H U, Kaiser U, Keimer B, and Botton G A 2014 *Phys. Rev. B* **90** 195140

[32] Yin X, Zeng S, Das T, Baskaran G, Asmara T C, Santoso I, Yu X, Diao C, Yang P, Breese M B H, Venkatesan T, Lin H, Ariando, and Rusydi A 2016 *Phys. Rev. Lett.* **116** 197002

[33] Nücker N, Pellegrin E, Schweiss P, Fink J, Molodtsov S L, Simmons C T, Kaindl G, Frentrup W, Erb A, and Müller-Vogt G 1995 *Phys. Rev. B* **51** 8529

[34] Chen C T, Tjeng L H, Kwo J, Kao H L, Rudolf P, Sette F, and Fleming R M 1992 *Phys. Rev. Lett.* **68** 2543

[35] Zhang X, Xu T, Shi R, Han B, Liu F, Liu Z, Gao X, Du J, Wang Y, and Gao P 2024 *Nano Lett.* **24** 13200

[36] Lanzara A, Bogdanov P V, Zhou X J, Kellar S A, Feng D L, Lu E D, Yoshida T, Eisaki H, Fujimori A, Kishio K, Shimoyama J I, Noda T, Uchida S, Hussain Z, and Shen Z X 2001 *Nature* **412** 510

[37] Xu X, Zhang S, Zhu X, and Guo J 2020 *J. Phys.: Condens. Matter* **32** 343003

[38] Nomura Y, Hirayama M, Tadano T, Yoshimoto Y, Nakamura K, and Arita R 2019 *Phys. Rev. B* **100** 205138

[39] Hao J J, Sun P H, Zhang M, Wu X X, Liu K, and Yang F 2022 *Chin. Phys. Lett.* **39** 067402

[40] Zhang X M and Li B 2022 *J. Solid State Chem.* **306** 122806

[41] Meier Q N, De Vaulx J B, Bernardini F, Botana A S, Blase X, Olevano V, and Cano A 2024 *Phys. Rev. B* **109** 184505

[42] Li Z and Louie S G 2024 *Phys. Rev. Lett.* **133** 126401

[43] Fu Y, Wang L, Cheng H, Pei S, Zhou X, Chen J, Wang S, Zhao R, Jiang W, Liu C, Huang M, Wang X, Zhao Y, Yu D, Ye F, Wang S, and Mei J W 2019 arXiv:1911.03177

[44] Zeng S, Tang C S, Yin X, Li C, Li M, Huang Z, Hu J, Liu W, Omar G J, Jani H, Lim Z S, Han K, Wan D, Yang P, Pennycook S J, Wee A T S, and Ariando A 2020 *Phys. Rev. Lett.* **125** 147003

[45] Li D, Wang B Y, Lee K, Harvey S P, Osada M, Goodge B H, Kourkoutis L F, and Hwang H Y 2020 *Phys. Rev. Lett.* **125** 027001

[46] Sahib H, Rosa F, Raji A, Merzoni G, Ghiringhelli G, Salluzzo M, Gloter A, Viart N, and Preziosi D 2024 arXiv:2410.16147

[47] Parzyck C T, Wu Y, Bhatt L, Kang M, Arthur Z, Pedersen T M, Sutarto R, Fan S, Pelliciari J, Bisogni V, Herranz G, Georgescu A B, Hawthorn D G, Kourkoutis L F, Muller D A, Schlom D G, and Shen K M 2024 arXiv:2410.02007

[48] Sun H, Huo M, Hu X, Li J, Liu Z, Han Y, Tang L, Mao Z, Yang P, Wang B, Cheng J, Yao D X, Zhang G M, and Wang M 2023 *Nature* **621** 493

[49] Zhu Y, Peng D, Zhang E, Pan B, Chen X, Chen L, Ren H, Liu F, Hao Y, Li N, Xing Z, Lan F, Han J, Wang J, Jia D, Wo H, Gu Y, Gu Y, Ji L, Wang W, Gou H, Shen Y, Ying T, Chen X, Yang W, Cao H, Zheng C, Zeng Q, Guo J, and Zhao J 2024 *Nature* **631** 531